

Synchronization in Electrically Coupled Neural Networks

Rajesh G. Kavasseri,

Department of Electrical and Computer Engineering

North Dakota State University, Fargo, ND 58105 - 5285

(email: rajesh.kavasseri@ndsu.nodak.edu)

Radhakrishnan Nagarajan

Institute of Aging, University of Arkansas for Medical Sciences

629 Jack Stephens Drive, Little Rock, AR 72205

Abstract

In this report, we investigate the synchronization of temporal activity in an electrically coupled neural network model. The electrical coupling is established by homotypic static gap-junctions (Connexin 43). Two distinct network topologies, namely: *sparse random network*, (*SRN*) and *fully connected network*, (*FCN*) are used to establish the connectivity. The strength of connectivity in the FCN is governed by the *mean gap junctional conductance* (μ). In the case of the SRN, the overall strength of connectivity is governed by the *density of connections* (δ) and the connection strength between two neurons (S_0). The synchronization of the network with increasing gap junctional strength and varying population sizes is investigated. It was observed that the network *abruptly* makes a transition from a weakly synchronized to a well synchronized regime when (δ) or (μ) exceeds a critical value. It was also observed that the (δ , μ) values used to achieve synchronization decreases with increasing network size.

Keywords : synchronization, electrical coupling, networks.

1 Introduction

Computational models of neural networks have been found to be useful in characterizing and validating hypotheses about how information processing occurs in real nervous systems. For example, a pulse coupled neural network (PCNN) model in [1] is capable of replicating temporal neural activity such as spindle waves, sleep oscillations and sustained spike synchrony. However, an important issue that affects the study of network dynamics is the choice of neural coupling, [1]. Neural coupling is accomplished by synapses which can be broadly classified in to (a) chemical synapses and (b) electrical synapses. While several studies consider the former type of coupling to be the preponderant way of intercellular communication, recent research has provided increasing molecular and functional evidence of the latter. More importantly, [2] and [3] suggest that neurons could also use electrical synapses to achieve intercellular communication. There have also been reports that emphasize the importance of electrical synapses in the temporal coordination of neuronal activity, [4], the generation of high frequency oscillations, [5] and the generation of oscillatory activity, [6].

The primary focus of this brief communication is to quantify the extent of synchronization in two general network models of electrically coupled neurons. The electrical coupling is achieved with the help of static homotypic gap-junctions (connexin-43). The choice of connexin 43 was based on a study [7] that presented molecular evidence for its presence in electrical connections between pairs of neurons in the visual cortex and hippocampal regions of the juvenile rat brain. However, the methods discussed are generic and can be extended to other static and dynamic gap-junctions. Two distinct network topologies namely fully connected network (FCN) and sparse random network (SRN) are used to establish the connectivity between the neurons. For example, Fig.1 illustrates a typical gap-junctional connection between a pair of neurons. In FCN, the gap-junctions are assumed to be exponentially distributed with mean conductance (μ). The exponential distribution was chosen as a possible means to capture the non-uniform distribution of gap-junctions in neuronal populations. In the case of FCN, the gap-junction strength between every pair of neurons is non-zero. An alternate approach to accomplish the distribution of gap-junctions is to assume a sparse-random network with a specified density

of connections (δ). Unlike the FCN, the coupling strength between any two pairs in SRN is either zero or one. SRN can be considered as a special case of FCN, where the gap-junctional conductance between a pair of neurons greater than a specified threshold is set to one and those lesser than the threshold are set to zero. Thus it might not be surprising to view SRN as a quantized version of the FCN.

While neurons are capable of exhibiting a rich set of firing patterns, we consider a population of *bursting* neurons in this study. Bursting behavior in neurons is considered important because bursts increase the reliability of synaptic transmission and provide a mechanism for selective communication between neurons, [8]. Planar bursters can be classified based on the bifurcation mechanism that leads to the corresponding burst activity (see [9] for a summary). In this study, we restrict all the bursters in the population to be of the “square-wave” or “fold-homoclinic” type. Burst synchronization in general, consists of two components (a) synchronization of spikes within a burst, and (b) synchronization between bursts, [18]. In order to minimize the contribution of the former, we studied the envelope $v_i^{env}, i = 1 \dots N$ of the bursts obtained by filtering the membrane potentials $v_i, i = 1 \dots N$. A representative burst and its corresponding envelope which approximates the duration of the burst is shown in Fig. 2.

In the present study, we show that increasing mean conductance (μ) and density of connections (δ) in the FCN and SRN result in increased synchronization as reflected by the synchronization index (M) (Sec. 3). The synchronization index (M) estimated on the original and their envelopes is discussed in (Sec.4). It is also shown that magnitude of the gap-junction strength (δ, μ) to achieve increased synchronization in FCN and SRN decreases with increasing population size.

2 The Model

In this study, we represent a network by three attributes, namely (a) individual neurons, (b) the connection between neurons and (c) the pattern of connectivity.

2.1 Individual Neuron : Model

While several models are available to represent a single neuron, we choose the recently proposed model by Izhikevich [1], [10], [11] which is described by a set of two coupled ordinary differential equations

$$\dot{v} = 0.04v^2 + 5v + 140 - u + I \quad (1)$$

$$\dot{u} = a(bv - u) \quad (2)$$

with auxiliary after-spike resetting given by

$$\text{if } v = +30\text{mV, then } \begin{cases} v \leftarrow c \\ u \leftarrow u + d \end{cases} \quad (3)$$

In Eqn.(3), the variable v represents the membrane potential of the neuron while u represents a recovery variable which accounts for the activation of K^+ ionic currents and inactivation of Na^+ ionic currents, [10]. The strength of the model is that it can exhibit firing patterns of every known type of cortical neuron for various choices of the parameters a, b, c and d , [10]. Moreover, the model is computationally superior to several other neuronal models, while being biologically plausible which makes it attractive for conducting large scale simulations and hence its choice in the present study. For a complete summary of the neuro-computational properties of this and other neuronal models, refer to [10].

2.2 Connections between neurons: Gap Junctions

Electrical synapses between neurons unlike chemical synapses, are fast and play a crucial role in the synchronization of neuronal activity. A gap-junction link consists of adjacent hemi-channels called connexons from neighboring cells. Each connexon being composed of proteins called connexins, whose conformational structure dictates their conductance. These junctions can be broadly classified into homotypic and heterotypic junctions. The variation of the junctional conductance with the transjunctional voltage is symmetric for homotypic junctions which is attributed to identical connexins. However, an asymmetric variation is characteristic of heterotypic junctions. In this study, we implicitly assume the junctions to be represented by the

homotypic Connexin 43 (Cx43-Cx43) which has been suggested to mediate neural communication, [7]. However, the methods to be discussed are generic and can be extended to other types of gap-junctions. Several models have been proposed in the past to model the dynamics of gap-junctions [12], [13], [14]. In the present study, we choose the contingent gating model [14], where the conductance of a channel between adjacent cells is given by,

$$g_n(v) = g_{res} + P_o(g_{max} - g_{res}) \quad (4)$$

$$P_o = \{1 + e^{a_0(-v-v_1)} + e^{b_0(v-v_2)}\}^{-1} \quad (5)$$

In the above expression, g_{res} represents the normalized residual conductance of the gap-junction, g_{max} the normalized maximum conductance, P_o the open probability of the gap-junction; a_0 , b_0 are the voltage sensitivity coefficients; v_1 , v_2 represent the voltages for half-maximal conductance. In Eqn.(5), v represents the transjunctional voltage which is the difference between the membrane potentials of the two cells connected by the gap-junction. Considering a homotypic channel (Cx43-Cx43) with identical gates (as suggested in [7]), the coefficients in Eqn.(5) have to satisfy $a_0 = b_0$ and $v_1 = v_2$, [14]. In this case, the variation of junctional conductance is symmetric with the transjunctional voltage which means $g_n(v) = g_n(-v)$. Further, the gap-junctional conductances are assumed to be static. This implicitly assumes the duration of the action potential to be much smaller than the changes in the gap-junctional conductance. The low-dimensional nature of the static contingent gating model makes it ideal for the present study, hence its choice. The values of the parameters in Eqn.(5) for the choice of homotypic connexon pairing (Cx43-Cx43) are presented in Table 1, [14]. With the present model, a different connexon pairing can be obtained by choosing the appropriate values of the parameters (g_{res} , g_{max} , a_0 , v_1 , b_0 and v_2) for that pairing from Table 1, [14]. While several factors affect the strength of gap-junctions, in the present study we represent the cumulative effect by a single parameter (S). Thus, the conductance of a gap-junctional channel between two neurons (i, j) in the network is given by

$$g_{ij} = S \times g_n(v), \quad v = (v_i - v_j) \quad (6)$$

A schematic representation of a pair of neurons (i, j) connected by a symmetric homotypic gap junction is shown in Fig. 1.

2.3 Pattern of Connectivity : SRN and FCN

In an ideal network, the neurons should be connected to accurately reflect the pattern of neural interconnections in the real brain. However, a lack of precise knowledge of the anatomical connectivity makes such a construction difficult in general. Here, we consider two models for the pattern of interconnections namely (i) a sparse random network (SRN) with fixed conductances through out the network and (ii) a fully connected network (FCN) where the conductances are exponentially distributed about a mean conductance μ . In the sparse random network model, we consider the gap-junctional strength (S) to be fixed between any two neurons, i.e. $S_{ij} = S_{ji} = S_0$ if the pair of neurons (i, j) are connected. The random network is created by generating a symmetric matrix W ($N \times N$) with density δ such that W has $(N^2\delta)$ non-zero entries. Here, the density δ of the SRN is defined as the (# of connections)/ N^2 . Then, a connection between a pair of neurons (i, j) is assigned only if $W(i, j) \neq 0$. If $W(i, j) = 0$, then no connection exists between neuron i and neuron j . Thus, the sparsity of the network is controlled by the parameter δ . In FCN, we assume a fully connected structure, that is, every pair of neurons in the network is connected. However, the connection strengths S_{ij} are assumed to be exponentially distributed about a mean strength μ . In both networks, note that the connections are made symmetric to enforce the bi-directional nature of gap-junctional couplings.

2.4 Overall Network Model

The overall network model is obtained by combining Eqns.(1, 2) for the neurons, Eqns.(4,5) for the gap junctional conductances and summing the contributions of synaptic current injections resulting from the appropriate network topology. In complex physiological systems such as neural assemblies, discrepancies in ionic exchanges between the neurons and their environment render the quantitative dynamics of individual neurons different from one another. Therefore, the neural population is modeled as set of N bursting neurons whose intrinsic parameters c_i, d_i and the thalamic input I_i are perturbed so that each neuron has a different burst duration and frequency. This is done by setting $a_i = 0.02, b_i = 0.2$ and $(c_i, d_i) = (-65, 8) + (15, -6)r_i$ where r_i is a random variable uniformly distributed in $[0,1]$. Thus, the dynamics of the i th neuron

in the network is described by

$$\dot{v}_i = 0.04v_i^2 + 5v_i + 140 - u_i + I_i + \sum_j g_{ij}(v_j - v_i) \quad (7)$$

$$\dot{u}_i = a_i(b_i v_i - u_i) \quad (8)$$

with auxiliary spike-resetting Eqn.(3)

3 Measures of Synchronization

Several measures have been proposed in the past [15] to determine the extent of synchronization in neural systems. These can be broadly categorized into linear and non-linear measures. While nonlinear measures may be more appropriate in the present context, their estimation can be quite challenging. In this report, we use pair-wise linear correlation ($0 \leq \rho \leq 1$) and Morgera's covariance complexity ($0 \leq C \leq 1$) [16] to quantify the extent of synchronization between the neurons.

3.1 Pairwise Correlations

The index (ρ_{ij}) between two neurons (i, j) is given by the linear correlation between their membrane voltages v_i, v_j respectively. For a system of N neurons, we obtain $P = {}^N C_2 = N(N-1)/2$, pair-wise dependencies. Statistically significant pair-wise dependencies were chosen as those whose p -values are lesser than a specified level of significance ($\alpha = 0.05$). The null hypothesis addressed is that there is no significant correlation between a given pair of neurons. It should be noted in the present study we have P pair-wise dependencies. In statistical literature, the choice of multiple testing correction such as Bonferroni correction is often recommended to minimize the false-positive rate. The adjusted significance is given by $\alpha_* = \alpha/P$. For example, in a ten element ($N = 10$) network, we have $P = 45$ and therefore, $\alpha_* = \alpha/P = 0.05/45 = 0.0011$. In the present study, the proportion of significant pair-wise correlations was determined as those whose p -values were lesser than α divided by P .

To determine whether the distribution of the (P) pair-wise dependencies across any two states of activity for the network is statistically significant (i.e. $\alpha = 0.05$), we used parametric (t-test) and non-parametric (Wilcoxon-ranksum) tests. Unlike the parametric test (t-test), non-parametric tests (Wilcoxon-ranksum) do not assume a normal distribution of the values and hence unbiased. However, non-parametric tests are based on ranks and not the original values, which is a limitation. Thus using a combination of parametric and non-parametric tests can minimize spurious conclusions that are an outcome of a particular test's assumption.

3.2 Morgera's Covariance Complexity

Morgera's covariance complexity is a linear measure and has been used recently for the analysis of brain signals [16], [17]. Here, we use this measure to define a synchronization index as follows. After simulating the activity of the network for a given interval (T) using a time step of $h = 0.5$ ms, the resulting $M = T/h$ discrete time points of the membrane voltages of the N neurons in the system is represented as a matrix $\Gamma_{M \times N}$ where ($N \ll M$). Singular value decomposition (SVD) of Γ yields N eigenvalues which explain the variance along the orthogonal directions in N -dimensional space. The normalized variance along the i th component is given by

$$\sigma_i = \frac{\lambda_i^2}{\sum_{i=1}^{i=N} \lambda_i^2}, \quad i = 1 \dots N \quad (9)$$

Then, Morgera's covariance complexity C is given by,

$$C = -\frac{1}{\log N} \sum_{p=1}^{p=N} \sigma_p \log \sigma_p \quad (10)$$

The synchronization index (M) is given by $M = (1 - C)$ and lies in the closed interval $[0,1]$. A minimum value of ($M = 0$) is obtained in the case of random behavior, whereas a maximum value ($M = 1$) is obtained in the case of perfect synchronization. However, due to external noise and nonlinear effects, the estimate of M deviates from these extreme values.

4 Simulation Results

The effect of increasing gap-junctional conductance on the synchronization was determined for a given population of neurons. Two distinct network topologies namely, FCN and SRN were considered. The synchronization is studied with increasing μ in case of FCN and increasing δ in case of the SRN. The synchronization index (M) was estimated on the actual membrane potentials ($v_i, i = 1 \dots N$) and their envelopes ($v_i^{env}, i = 1 \dots N$). The choice of the envelopes was in order to minimize the effect of spikes within bursts on the synchronization index. In order to determine the effect of varying population size on the synchronization, we investigated three different populations namely ($N = 10, 50$ and 100).

The estimate of M determined on 20 independent trials with varying gap-junctional conductance and population sizes is shown in Figure 3. In the case of FCN, the synchronization index saturates around ($M \sim 0.9$) for parameter ($\mu = 40, 20$ and 5) and population sizes ($N = 10, 50$ and 100), Figure 3 (top). An abrupt transition in the synchronization index is observed at a critical density of $\delta \sim 0.2$ for all three network sizes, Fig.3 (bottom). To generate a quantized version of the FCN, we constructed SRN, where the connection strengths S_0 was fixed at $40, 20$ and 5 for populations ($N = 10, 50$ and 100) respectively. While the connection strength (S_0) is fixed between connected pairs of neurons, their density δ (Sec 2.2, Eqn.(6)) which controls the number of connections is gradually increased. It should be noted that while $\delta \in [0, 1]$ is a normalized measure of network density, the actual number of connections ($N^2\delta$) varies in the range $[0, N^2]$ for a network of size N . For clarity, we show the variation of the synchronization index (M) with respect to ($S_0 \times \delta = S_0 \times \# \text{number of connections} / N^2$) which we shall denote by \bar{S} . Note that \bar{S} quantifies the average connection strength of the SRN. As with the case of FCN, we find the network synchronizes with increasing \bar{S} . The synchronization is achieved at a magnitude similar to FCN. As expected, increasing (μ) or \bar{S} leads to increasing synchronization of the network. Interestingly, the magnitude of the parameter (μ, \bar{S}) required to achieve synchronization decreases with increasing population size in the FCN and SRN respectively, Fig. 3.

While the estimate of M obtained on the membrane potentials and their envelopes converge

to a similar value with increasing (\bar{S} or μ), the abrupt transition is better reflected by those estimated on the envelopes, Figure 3. This behavior was consistent varying population sizes ($N = 10, 50$ and 100).

Parametric (t-test) and non-parametric (Wilcoxon-ranksum) statistical tests were used to determine statistically significant change ($\alpha = 0.05$) in the distribution of the pair-wise linear correlation before and after synchronization. The parameters ($\bar{S} = 0$) and ($\mu = 0$) were used to represent the networks SRN and FCN before synchronization. The (μ) and (\bar{S}) values after synchronization for the various population sizes ($N = 10, 50$ and 100) were chosen as ($\mu, \bar{S} = 40, 20$ and 5) from Figure 3. The distribution of the pair-wise linear correlations before and after synchronization for the various population sizes for FCN and SRN is shown in Figure 4. The distributions were statistically significant after Bonferroni correction. This result was consistent for all three population sizes.

5 Conclusions

In this brief report, we studied the synchronization of temporal activity in a neural network with electrical synaptic couplings. The neuronal parameters were randomized to yield different burst durations and frequencies but constrained to restrict their behavior to *square-wave* type bursting. The electrical couplings were established by a generic model to represent the homotypic, bi-directional and static gap-junctional couplings formed by Connexin-43. Two network topologies namely, (a) sparse random network (SRN) and (b) a fully connected network (FCN) were used to model the pattern of connectivity. The overall mean conductance of the network was governed by δ the density of interconnections and S_0 the fixed connection strength in SRN, and μ the mean conductance in FCN. Synchronization of burst activity was quantified using (a) the distribution of pairwise linear correlations and (b) Morgera's covariance complexity. Numerical simulations were conducted to study the synchronization of the network with increasing coupling strength and varying population sizes.

We observe that in both networks, an increase in the mean gap junctional coupling strength

(\bar{S}, μ) results in an increased degree of synchronization. In addition, we observe that the network exhibits an *abrupt* transition from a poor to highly coordinated regime at a critical value of these parameters. Further, while the magnitude of the parameter μ required to achieve synchronization decreases with increasing population size in FCN, the abrupt transition to increased synchronization seems to occur at a network density of $\delta \sim 0.2$ for all three network sizes in case of the SRN.

Our results in general, support the prevailing notion that gap-junctions promote synchrony in large neural assemblies. The computational studies show that in addition to coupling strength of the gap-junctions, the density of their connections in the two topologies (SRN and FCN) also plays an important role in promoting synchrony. Moreover, the results suggest the existence of *critical* parameters at which a large neural network could tune, or transition to a high degree of synchronization.

References

- [1] E. M. Izhikevich, Simple Model of Spiking Neurons, IEEE Trans. on Neural Networks, vol. 14, **6**, Nov. 2003, pp :1569 - 1572.
- [2] M. V. L. Bennett, Seeing is relieving: electrical synapses between visualized neurons, Nature Neuroscience, **3**, 2000, pp : 7-9.
- [3] M. Galarreta and S. Hestrin, A network of Fast-Spiking Cells in the Neocortex Connected by Electrical Synapses, Nature (London), **402**, 1999, pp: 72-75.
- [4] P. M. Metzer and Y. Yarom, Electrotonic Coupling Interacts with Intrinsic Properties to Generate Synchronized Activity in Cerebellar Networks of Inhibitory Interneurons , J. Neuroscience, **19**, 1999, pp : 3298 - 3306.
- [5] A. Draguhn, R. D. Traub, D. Schmitz, and J. G. R. Jefferys, Electrical coupling underlies high-frequency oscillations in the hippocampus *in vitro*, Nature, **394**, 1998, pp : 189- 192.
- [6] J. J. Chrobak and G. Buzsaki, High-Frequency Oscillations in the Output Networks of the Hippocampal-Entorhinal Axis of the Freely Behaving Rat , J. Neuroscience, **16**, 1996, pp : 3056-3066.
- [7] L. Venance, A. Rozov, M. Blatow, N. Burnashev, D. Feldmeyer and H. Monyer, Connexin expression in electrically coupled postnatal rat brain neurons, Proc. Nat. Acad. Sci, vol. 97, **18**, Aug 2000, pp : 10260 - 10265.
- [8] E. M. Izhikevich, N. S. Desai, E. C. Walcott and F. C. Hoenstaedt, Bursts as a unit of neural information : selective communication via resonance, Trends in Neurosciences, vol. 26, **no. 3**, March 2003, pp : 161-167.
- [9] E. M. Izhikevich, Neural Excitability, Spiking and Bursting, Intl. Journal of Bifurcations and Chaos, 10, 2000, pp : 1171-1266.
- [10] E. M. Izhikevich, Which Model to Use for Cortical Spiking Neurons ?, IEEE Trans. on Neural Networks, vol.15 no.5, 2004, pp : 1063- 1070.

- [11] E. M. Izhikevich, *Dynamical Systems in Neuroscience, The geometry of excitability and bursting*, (in preparation) for Springer-Verlag.
- [12] A. L. Harris, D. C. Spray and M. V. L. Bennett, Kinetic Properties of voltage dependent junctional conductance, *J. Gen. Physiology*, 77, 1981, pp : 95 - 117.
- [13] Vogel and Weingart, Mathematical model of vertebrate gap junctions derived from electrical measurements on homotypic and heterotypic channels, *J. Physiology*, 510.1, 1998, pp : 177-189.
- [14] Y. Chen-Izu, A. P. Moreno and R. A. Spangler, Opposing gates model for voltage gating of gap junction channels, *American J. Physiology (Cell Physiology)*, 281, 2001, pp : C1604-C1613.
- [15] R. Q. Quiroga, A. Kraskov, T. Kreuz and P. Grassberger, Performance of different synchronization measures in real data : A case study on electroencephalographic signals, *Phy. Rev. E*, vol. 65, 2002, pp: 0419030 : 1-13.
- [16] S. S. Morgera, Information theoretic complexity and relation to pattern recognition, *IEEE Trans. on Systems, Man and Cybernetics*, 15, 1985, pp : 608 - 619.
- [17] T. A. A. Watanabe, C. J. Cellucci, E. Kohegyi, T. R. Bashore, R. C. Josiassen, N. N. Greenbaum and P. E. Rapp, The algorithm of multichannel EEG is sensitive to changes in behavior, *Psychophysiology*, 40, 2003, pp : 77-97.
- [18] Eugene M. Izhikevich, “Synchronization of Elliptic Bursters”, *SIAM review*, vol. 43, **no. 2**, 2001, pp : 315 - 344.

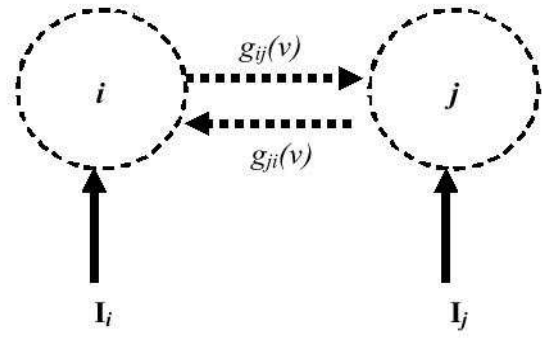


Figure 1: A pair of neurons coupled by a symmetric homotypic gap junction such that $g_{ij}(v_{ij}) = g_{ji}(v_{ji})$ where $v = v_{ij} = -v_{ji}$ is the transjunctional voltage. The tonic activation currents are I_i and I_j for neurons i and j respectively.

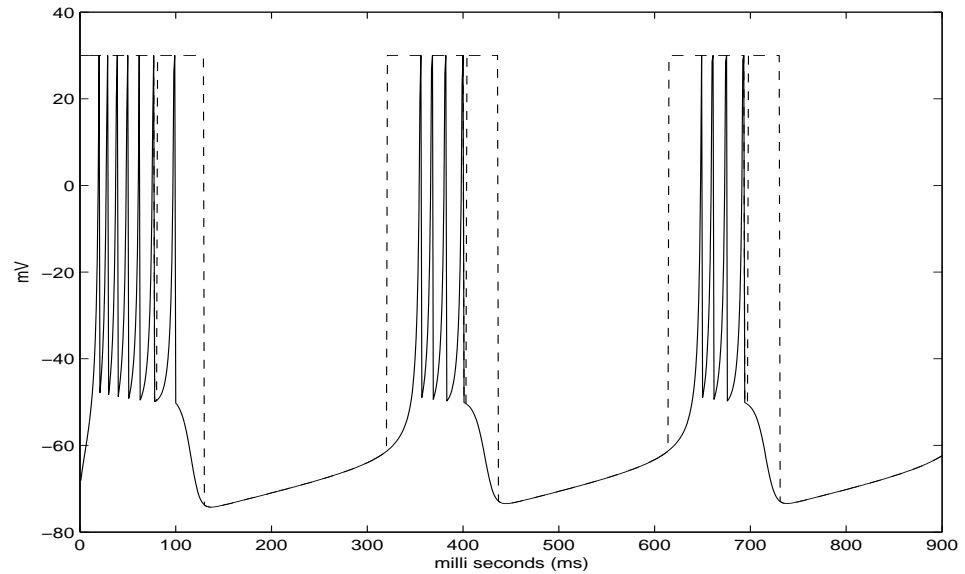


Figure 2: A representative burst (solid line) and its corresponding ‘envelope’ (dotted line). The envelope approximates the duration of the burst.

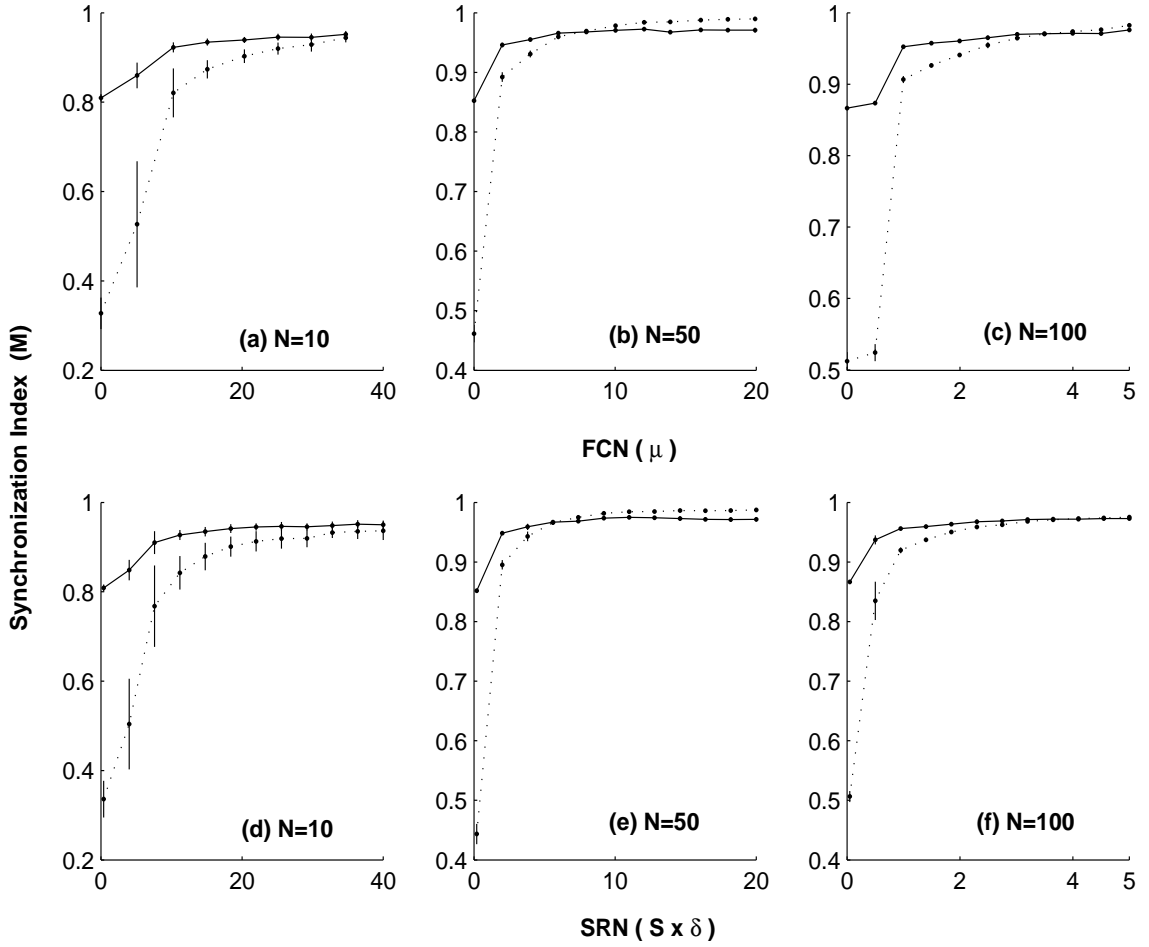


Figure 3: Variation of the synchronization index (M) with parameters μ and δ for the fully connected network (top) and sparse random network (bottom). The vertical lines represent the variance about the mean value (dots) for twenty independent trials. Estimates of (M) obtained on the original waveforms $v_i, i = 1 \dots N$ (solid lines) and the envelopes $v_i^{env}, i = 1 \dots N$ (dotted lines) for three different population sizes $N = 10, 50$ and 100 is also shown.

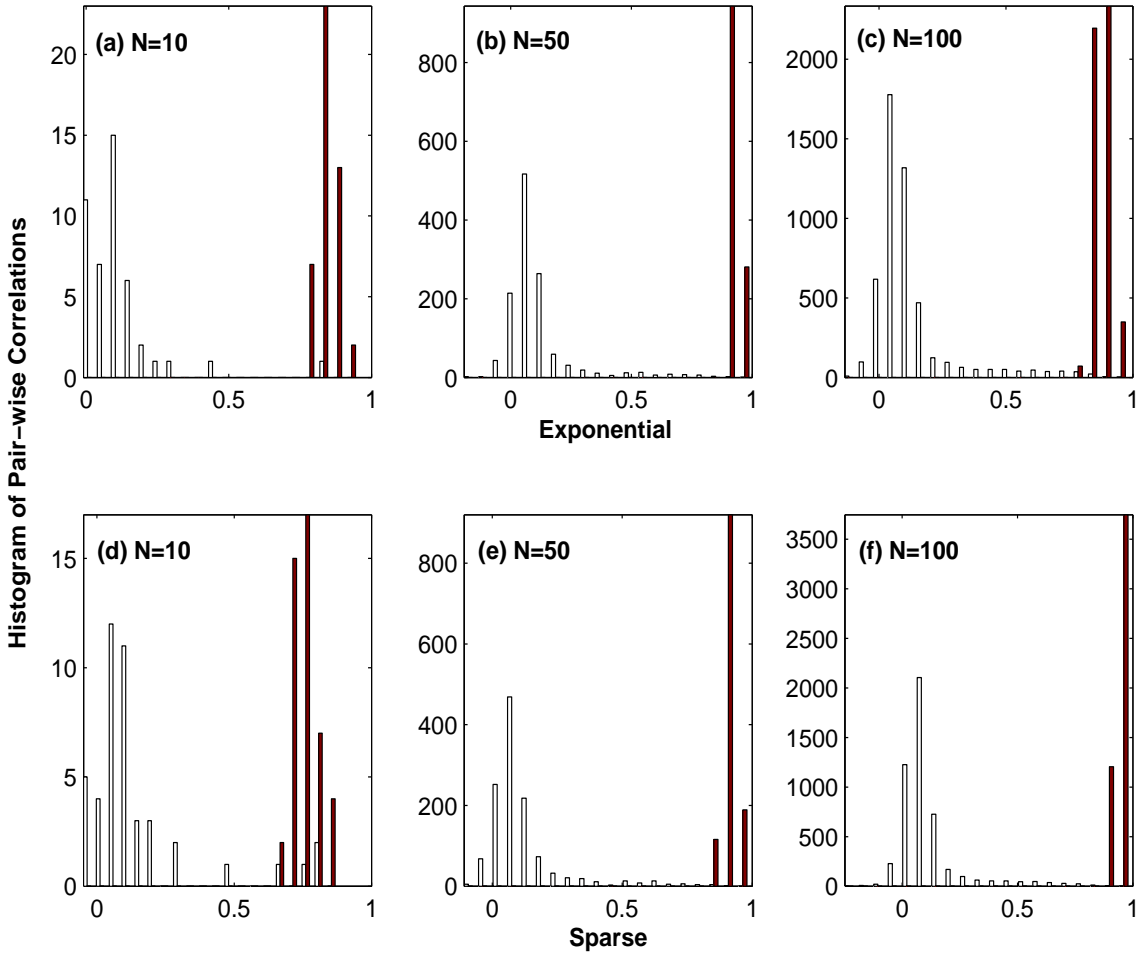


Figure 4: Distribution of the pair-wise linear correlations estimated before and after synchronization for FCN (top) and SRN (bottom). Pair-wise correlation before synchronization for FCN and SRN were obtained by setting $(\mu = 0)$ and $(\bar{S} = 0)$, represented by hollow bars. Distribution of the pair-wise correlation after synchronization for parameters $(\mu = 40, 20$ and 5 , top) and $(\bar{S} = 40, 20, 5$, bottom) for population sizes $(N = 10, 50, 100)$ is shown in (a, b, c) and (d, e, f) respectively.